Visual Analysis of Spatio-temporal Relations of Pairwise Attributes in Unsteady Flow – *Supplemental Document*

Marzieh Berenjkoub, Lei Zhang, Rodolfo Ostilla Monico, Robert S. Laramee, and Guoning Chen

In this supplemental document, we provide additional results for our correlation and dependency measurement and visualization of pairwise attributes in unsteady flow.

1 Correlation Glyphs

To show the local properties of the correlation field at a given position **p**, we employ a disk glyph. The disk is divided into two hemi-circles. Each hemi-circle visualizes the values of the specific attribute measured at the points within the spatio-temporal kernel K (centered at **p** with spatial size r and temporal length h). Specifically, we represent the attribute values of the sampled points in K as a 1D sequence given certain ordering of these points. As long as the ordering is consistent for the two hemi-circle, their respective trends can provide an intuitive description of the ST_LCC correlation measured at **p**. A heat map color coding is used for the glyph with calibrated ranges to make their gradient discernible.

These correlation glyphs can either be placed at fixed locations in space for the user to examine the temporal evolution of attributes involved in an Eulerian sense (Figure 1a), or be associated with flow particles and be advected over time to inspect their Lagrangian behavior (Figure 1b). Specifically, in Figure 1b, two pathlines are seeded at the center of a vortex (upper left pathline) and at the outer layer of a vortex (lower right), respectively. The two pathlines are colored based on the ST_LCC values for the gradient-based similarity of vorticity (A_1) and Jacobian determinant (A_6) over time as described earlier. The pathline seeded at the vortex center region exhibits relatively constant color mapping. At the same time, the correlation glyphs sampled along this pathline show similar trends of the two attributes over time, verifying the stable correlation. Similarly, for the pathline seeded at the outer layer of a vortex, the correlation glyphs intuitively illustrate the different trends of the two attributes, reflecting the varying colors along this pathline. Similarly, a glyph can be designed to display the distribution of the pairwise attributes to explain the MI results.

Figure 2 provides the aforementioned glyph and pathline visualization on the HCCI data. From this visualization, we see that those pathlines seeded from the boundary layer of vortices are in a helix shape (Figure 2b) and changing the color over time, while those started at the center area of vortices are almost straight and with little change of color over time. Note that the color pattern of each glyph in (a) represents the trend of the corresponding attributes along the pathline where the glyph is placed.

• Marzieh Berenjkoub, Lei Zhang, Rodolfo Ostilla Monico and Guoning Chen are with the University of Houston. E-mails: mberenjkoub@uh.edu, zhanglei.later@gmail.com, rostilla@central.uh.edu, and gchen16@uh.edu.

• Robert S. Laramee is with Swansea University. E-mail:r.s.Laramee@swansea.ac.uk

Manuscript received xx xxx. 201x; accepted xx xxx. 201x. Date of Publication xx xxx. 201x; date of current version xx xxx. 201x. For information on obtaining reprints of this article, please send e-mail to: reprints@ieee.org. Digital Object Identifier: xx.xxxx/TVCG.201x.xxxxxxx

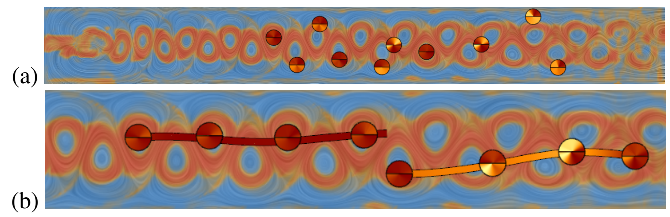

Fig. 1: Correlation glyphs on sampled spatial locations at the first time step (a) and along the sampled pathlines over time (b) of the 2D flow behind a cylinder simulation. Each glyph visualizes the attribute values within a kernel (r=3 and h=250) centered at the glyph location. A heat map color scheme is used to convey the attribute information.

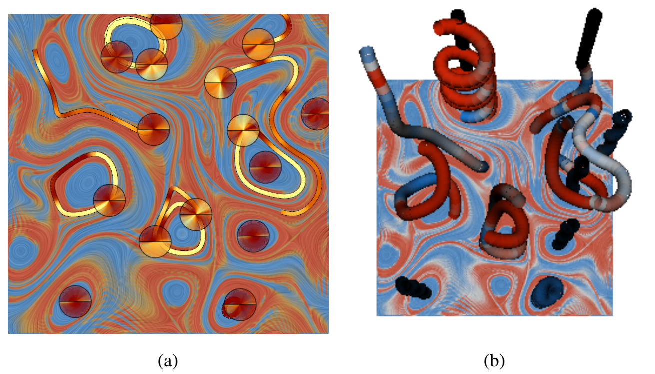

Fig. 2: Glyph and pathline visualization for ST_LCC of acceleration and Q for HCCI.

2 Remarks on conditional entropy

Consider two attributes A_1 and A_2. The entropy $H(A_1)$ within a kernel K measures the variation of the values that A_1 has within K (i.e., the more different values, the larger the $H(A_1)$ is). On the other hand, the entropy $H(A_2 \mid A_1)$ measures the amount of uncertainty of attribute A_2 given the known probability of the values of attribute A_1. That is, if the values (and their probability distribution) of A_2 can be estimated from A_1, $H(A_2 \mid A_1)$ will be low. This intuition may be applied to study the casual relation between pairwise attributes. Note that $H(A_2 \mid A_1)$ is usually not equal to $H(A_1 \mid A_2)$. Thus, if $H(A_2 \mid A_1) < H(A_1 \mid A_2)$, one may consider A_1 as an indicator of A_2, but not the other way around. For example, consider two attributes λ_2 and *Norm* in a flow. We compute its $H(Norm|\lambda_2)$ (Figure 3a) and $H(\lambda_2|Norm)$ (Figure 3b), respectively. We see that in most regions, *Norm* is dependent on λ_2, while λ_2 is less dependent on *Norm*, since $H(Norm|\lambda_2) < H(\lambda_2|Norm)$. This is expected, as regions with strong vortical flow result in larger norm of the Jacobian, while the inverse is not always true.

3 Additional 2D Results

In the following, we provide additional results on a number of 2D unsteady flow.

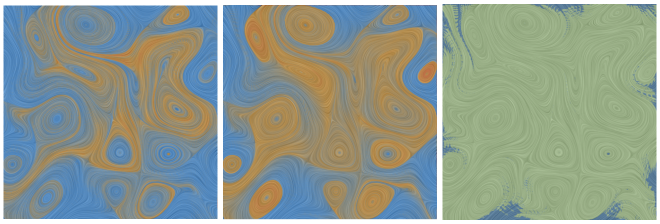

(a) $H(A_7|A_3)$ (b) $H(A_3|A_7)$ (c) Comparison.

Fig. 3: The comparison of conditional entropy for the norm of the Jacobian (A_7) vs. λ_2 (A_3). Blue-white-red color coding is applied to (a) and (b), while for (c), light green indicates $H(A_7|A_3) < H(A_3|A_7)$ while blue means $H(A_3|A_7) < H(A_7|A_3)$.

2D flow past cylinder Figure 4 shows the results using various MI and correlation measurements for the norm and λ_2 on the 2D flow past cylinder data. From these results, we see that $H(Norm|\lambda_2)$ highlights the boundary of vortices which shows that norm is a good attribute for highlighting the boundary layer of vortices, while $H(\lambda_2|Norm)$ focused on the whole shape of vortex which indicates that λ_2 better highlights the center areas of vortices. Figure4c shows the ST_MI for norm and λ_2. From the result, we see that these two attributes are highly dependent on each other at the center areas of vortices, which matches with two previous results for conditional probability and is expected based on the MI formula. Figure 4d shows ST_LCC between these two attributes. As we can see, it only highlights region outside of the vortices and cannot differentiate the boundary of the vortices anymore. This is a good example of non-linear relation between two attributes, which can only be revealed by MI.

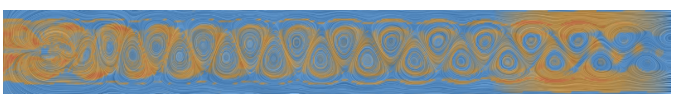

(a) $H(Norm|\lambda_2)$

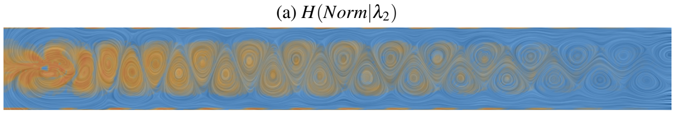

(b) $H(\lambda_2|Norm)$

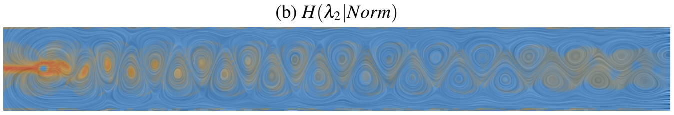

(c) Lagrangian ST_MI

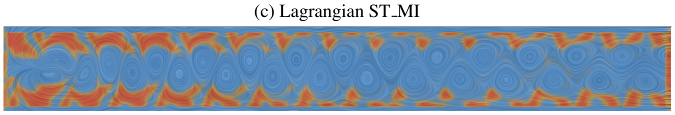

(d) ST_LCC

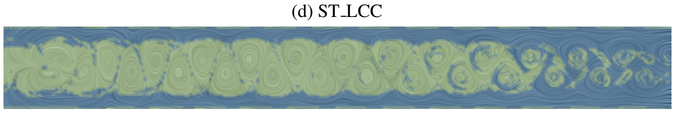

(e) Comparison between $H(Norm|\lambda_2)$ and $H(\lambda_2|Norm)$

Fig. 4: Different MI and correlation measurements between norm (A_7) and λ_2. Blue-white-red color coding is used for (a)-(d), while for (e), green indicates that $H(Norm|\lambda_2) < H(\lambda_2|Norm)$.

Figure 5 visualizes the ranking-based segmentation on the 2D flow past cylinder. More specifically, Figure 5a shows the result of the ranking based on all possible pairs of attributes. Different colors correspond to different top-ranked pairs of attributes. From this segmentation result, we see that the norm of the Jacobian, *Norm*, and shearing are dominant in most of the non-vortex regions which is shown by yellow color. As we already know that the dominant characteristic of this flow is the karman vortex street, we concentrate on the three relevant attributes, acceleration, Q and local shear rate for the ranking. Figure 5b shows this ranking-based segmentation. From this result, we can see that the acceleration and Q are highly correlated at the boundary layer of vortices (colored by blue), while the shearing and accelerating (colored in dark green) are dominating in the center of the vortex. The rest of the domain is dominated by shearing and Q, as both attributes have small values there. This ranking strategy provides an overview of the dominant flow dynamics (e.g., rotational versus stretching or shearing) in different flow regions.

(a) Ranking-based segmentation of all pairs of attributes.

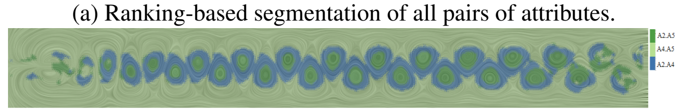

(b) Ranking-based segmentation between acceleration and Q and shearing.

Fig. 5: Ranking of ST_LCC value of attributes for cylinder flow. As we can see the pair of acceleration and Q is ranked top in vortex boundary, while the pair of acceleration and shearing is ranked top at the center of vortexes. Kernel size $r = 3$ and $h = 250$ is used. Different colors indicate different pairs of attributes whose ranking is the highest at specific locations.

HCCI data Figure 6 shows the ranking-based segmentation for the HCCI data. In particular, Figure 8a shows the ranking results between all pairs of attributes. Similar to the results of the 2D cylinder flow, *Norm* and shearing (brown color) are dominant in non-vortex regions. Figure 8c compares the Lagrangian ST_LCC for three pairs of attributes, i.e., *norm* and shearing, acceleration and Q, vorticity and Q, and Figure 6c compares the results between the first two pairs of attributes in the previous image. It shows that the pair of acceleration and Q always highlights the boundary of vortices, when compared to *Norm* and shearing.

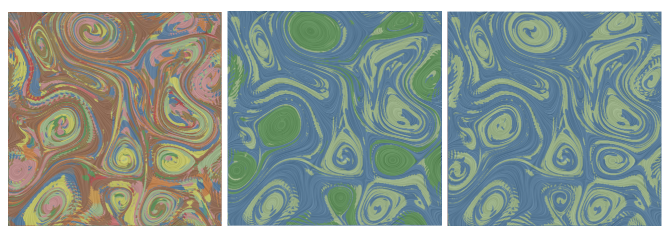

(a) (b) (c)

Fig. 6: The illustration of the ranking between (a) all pairs (21 pairs) of attributes, (b) A_2 and A_4, A_5 and A_1, A_3 and A_5, (c) A_2 and A_4 and A_5 and A_7 with kernel size equals to 3×100.

2D axisymmetric vortex ring Figure 7 compares the ST_LCC and ST_MI results using the acceleration and Q on the vortex ring data considering the kernel size of r=3, h = 40, and $\tau = 0.05$. From the result, we see that ST_LCC highlights the center of the primary vortex before hitting the wall, while the ST_MI field puts emphasis on the secondary vortex arises on the right after the vortex ring hitting the wall.

Figure 8 shows the pathline visualization of the axisymmetric vortex ring impact simulation. The pathlines are seeded at different regions where the primary vortex swept through before hitting the wall and creating the secondary vortex. Those pathlines are colored based on the ST_LCC of the vorticity and Q measured along with the advected particles. The two plots in (b) and (c) show the two attribute behaviors within a kernel (or a local neighborhood) located at vortex region. From

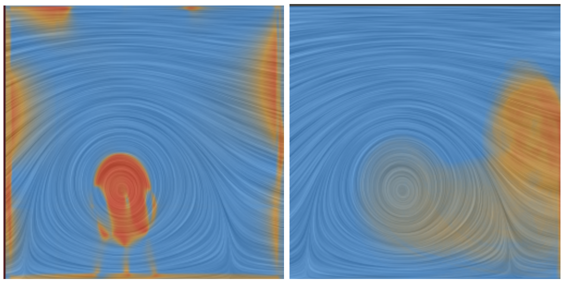

(a) (b)

Fig. 7: ST_LCC and ST_MI results for acceleration and Q of the 2D axisymmetric vortex ring data. The spatial kernel size is 3 and the temporal one is 40.

this visualization, we can easily identify pathlines seeded in the outer layer of the vortex, whose associated correlations of the two attributes exhibit large fluctuation (i.e., unstable). Those pathlines seeded near the vortex center have lower fluctuation. Also, due to the movement of vortex, many parts of the pathlines doesn't have value (i.e., white color). The reason is that the size of the vortex is changing during its movement and its impact with the wall, causing some pathlines seeded in the outer layer of the vortex to exit the vortex region. As the attribute values outside the vortex is negligible, our filtering mechanism used to remove areas with small attribute values will assign no value for the portion of those pathlines that is outside of the vortex region.

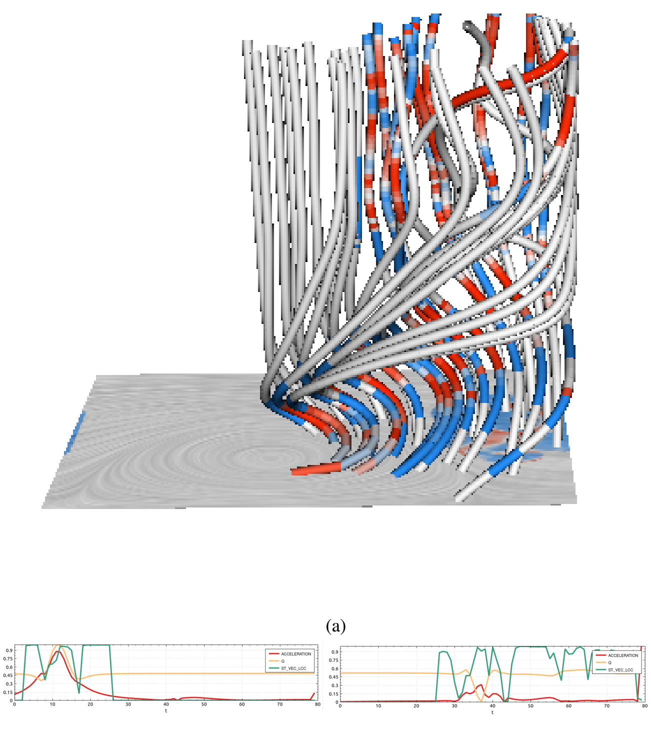

(a)

(b) (c)

Fig. 8: Sampled pathlines color coded by ST_LCC of vorticity and Q for the 2D axisymmetric vortex ring simulation. The two plots shown in (b) and (c) illustrate the temporal behaviors of the two attributes within two sampled kernels located at two pathlines, respectively.

Ocean current Figure 9 provides the ST_LCC result between the temperature and vorticity for the large-scale ocean current simulation. The spatial kernel size is r = 5 and the temporal one is h = 50 (with $\tau = 0.004$). As we see, the relation between temperature field and vorticity is very complex. There are other parameters and attributes which are playing a role, such as, salinity concentration and Earth's rotation. What is visualized in this result are the main circulations/gyres, i.e. the Gulf stream, the equatorial circulation, the Antarctic circulation, etc.. It is hard to say if there is a direct relationship between these two attributes since the relationship is quite complex.

4 Additional 3D Results

In the following, we provide more results using our framework on a number of 3D data.

3D Isabel simulation Figure 10 provides the spatial LCC (S_LCC) of the attributes acceleration and shearing on the 3D Isabel simulation. In this example, we compare the effect with or without normalizing the attribute values during the computation of LCC. The normalization helps to constrain the value ranges of the two attributes into $[-1, 1]$. From this comparison, we see that normalization helps to reduce the noise especially when some pathlines cover a large area of the domain in reality, among which only a small portion corresponds to the hurricane and has meaningful values. See a similiar example in Figure 8. Also, the correlation patterns between acceleration and Q vs. acceleration and shearing show opposite behaviors in vortex regions (i.e., the patterns of these two correlation fields complement each other to some extend).

3D vortex tube simulations

Figure 11 shows the pressure, vorticity and the spatial correlation between them for the vortex tube simulation with elliptical instability. The results show that the pressure and vorticity are negatively correlated almost everywhere in the tube region. This is because the minimum of pressure and the maximum of vorticity are in the center of the vortex (as shown in Figure 11a and b).

Figure 12 shows the effect of applying thresholding to the correlation computation on the tube dataset. Since we use standard deviation in denominator in our metrics, for those datasets such as tube data, hurricane Isabel or vortex ring where vortices only exist in a small region of the flow domain and move through the whole domain, the covariance values are very low for those regions without vortical flow (i.e., with only laminar flow). That causes the artifacts in our results shown in Figure 12c. Setting a threshold to remove those areas will yield a much cleaner and more meaningful visualization for those datasets (see Figure 12d, compared to c).

In addition to thresholding and filtering the empty region, we also consider the effect of normalization in our metrics. Normalization is essential for MI computation, especially when we use uniform bins. For LCC computation, normalization is not as useful as MI, but it could still help suppress some artifacts as mentioned above in places with small attribute values, leading to a cleaner visualization with the effect similar to the above thresholding. Normalization also helps to filter those regions where the attribute values appear to be constant (i.e., the corresponding 1D plot of the attribute is flat). This flat (or constant) configuration will result in very small (almost zero) standard deviation, leading to abnormally large correlation values, thus, artifacts.

Figure 13 shows the result of S_LCC and ST_MI between acceleration and Q using normalization. Figure 13a and b visualize the two attributes. We can see that acceleration is almost zero in the center of each vortex tube, while Q has the highest value there. The S_LCC results highlight the opposite relation of these two attributes in the center of each vortex and a positive one at the outer layer of vortices. Figure13d shows the MI results, which highlights the general path that vortex center swept through. Also, we can see the effect of normalization in both S_LCC and ST_MI results, and how the normalization helps to highlight the main region of vortical flow.

Figure 14 shows a comparison between the Lagrangian and Eulerian ST_MI for acceleration and vorticity. The total number of time frames for this dataset is 25, and we consider the temporal kernel, h = 20. In the Lagrangian ST_MI, the dye and vorticity are highly dependent on each other at the vortex cores, because there is no additional vorticity generated anywhere, and the dye tracks the vorticity well. The Eulerian

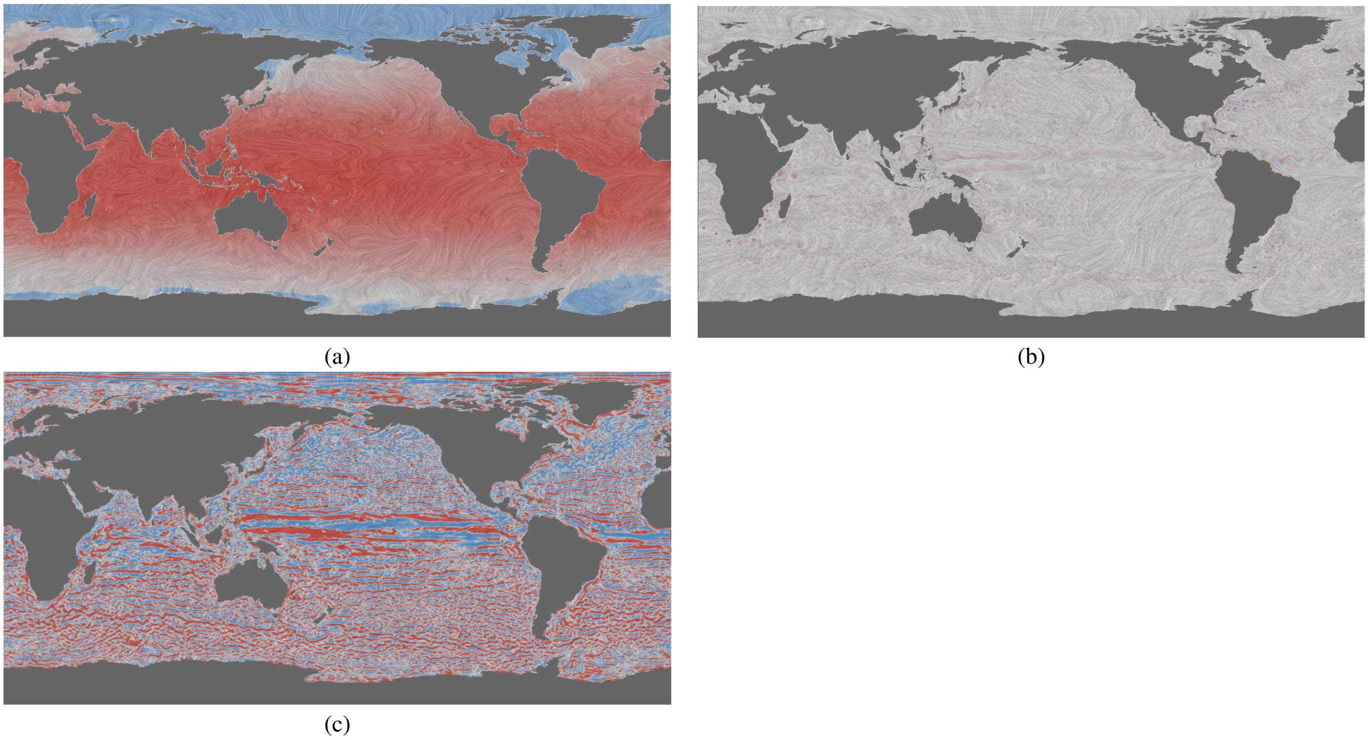

Fig. 9: The ST_LCC linear correlation (c) of the temperature (a) and vorticity (b) of the large ocean simulation data with a spatio-temporal kernel size 5×50. The blue-white-red color scheme is used to highlight the different characteristics of attribute correlation and dependency.

result is similar to the Lagrangian one, except that it shows that the two vortices move in the horizontal direction due to self-induction, and then reconnect on the left side of the image.

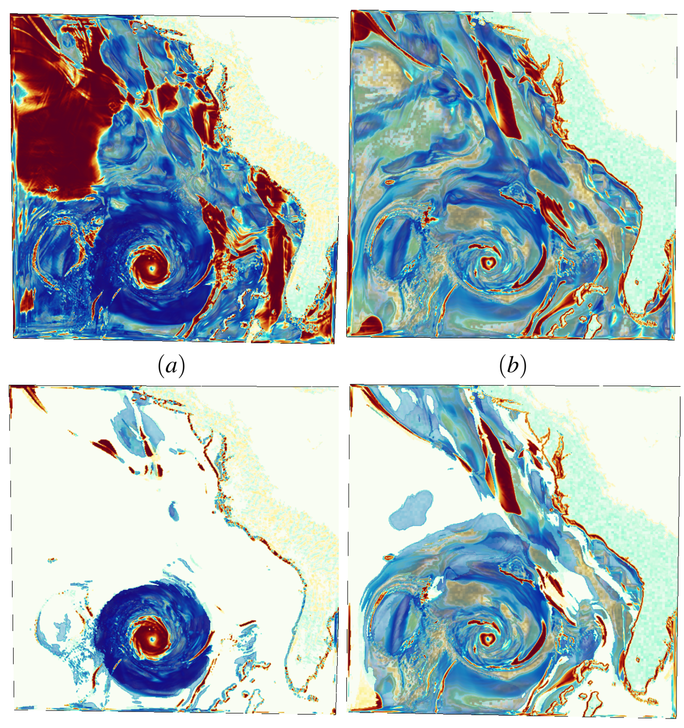

Fig. 10: The effect of attribute normalization on spatial LCC for the hurricane Isabel simulation. (a) and (b) are generated without normalization. (c) and (d) are obtained using normalization. The left results are spatial LCC for acceleration and Q, while the right results are spatial LCC between acceleration and shearing.

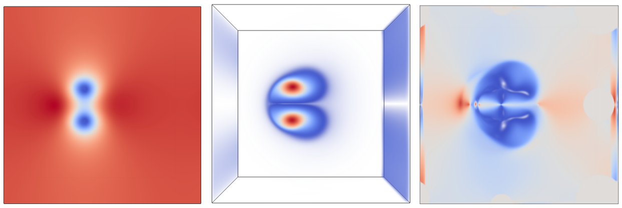
(a) (b) (c)

Fig. 11: The Spatial correlation (c) for pressure (a) and vorticity (b) for the Tube data. The spatial kernel size is 3.

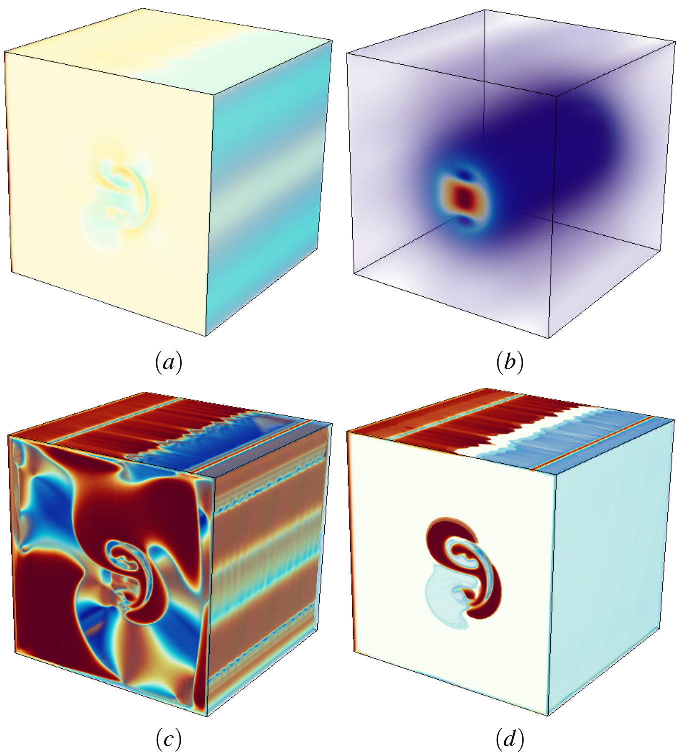
(a) (b) (c) (d)

Fig. 12: The effect of thresholding in spatial LCC (c) of divergence(a) and shearing(b) captured at the first frame of the elliptic tube simulation. The divergence values are really small, which caused some artifacts in the LCC computation. In order to remove those artifacts, we set a threshold for the co-variance of each attribute(d). The threshold value we used is e^{-12}.

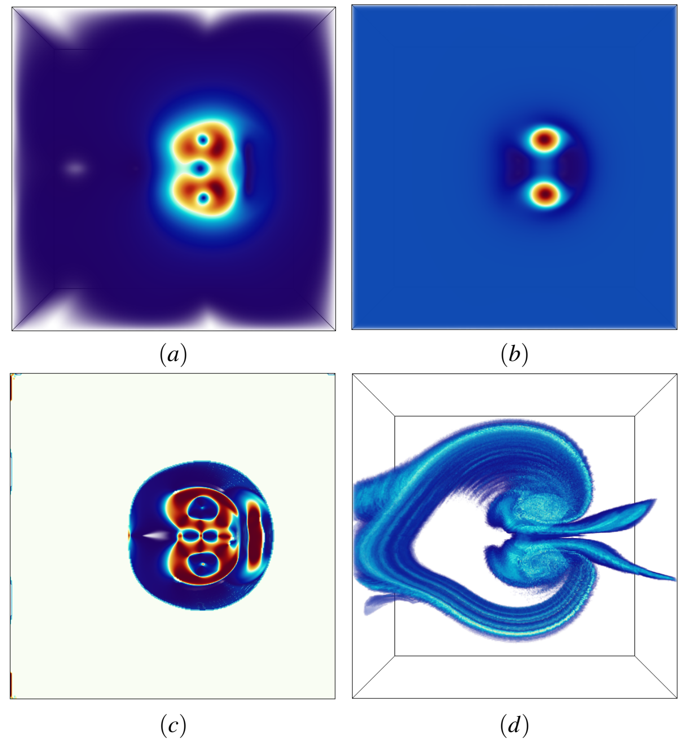
(a) (b) (c) (d)

Fig. 13: Spatial LCC (S_LCC) (c) and mutual information ST_MI (d) between acceleration (a) and Q (b) at the first frame of the elliptic tube data. The S_LCC result (c) shows that these two attributes are negatively correlated in the center and positively correlated in the boundary of each vortex tube. The ST_MI result (d) highlights the path that the center of each tube is sweeping through. The temporal kernel size for ST_MI is h = 20 and $\tau = 0.1$. The spatial kernel size is 3 for both results.

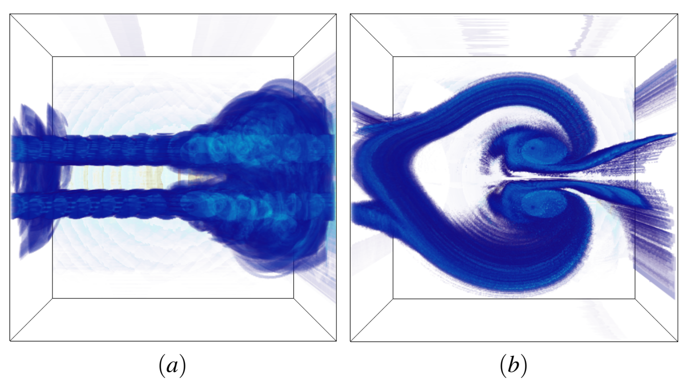
(a) (b)

Fig. 14: Comparing Eulerian (a) and Lagrangian (b) ST_MI for dye and vorticity of the elliptic tube simulation.